CFD modelling of drop formation in a liquid-liquid system

Timgren, Anna; Trägårdh, Gun; Trägårdh, Christian

Published in:
6th International Conference on Multiphase Flow

2007

6th International Conference on Multiphase Flow,
ICMF 2007, Leipzig, Germany, July 9 – 13, 2007

CFD modelling of drop formation in a liquid-liquid system

Anna Timgren, Gun Trägårdh and Christian Trägårdh

Lund University, Department of Food Technology, Engineering and Nutrition
P.O. Box 124, SE-221 00 Lund, Sweden
E-mail: Anna.Timgren@food.lth.se

Keywords: Interfacial shear, Emulsification, VOF

Abstract

The formation of an oil drop from a single capillary in a continuous phase flowing perpendicular to the capillary opening has been studied numerically. The shear stress at the interface of the forming drop, the angular velocity inside the drop and the pressure field around the drop have been determined in a cross section of the drop formation area. The results show a maximum pressure in the continuous phase near the stagnation point and a maximum shear stress in both phases nearer the top of the forming drop. The lowest pressures were found behind the top of the drop, where the surrounding flow starts to separate from the interface of the drop. The shear stress outside the drop causes a drag which, together with the drag originated from the pressure field around the drop, promotes drop detachment.

1 Introduction

A better understanding of drop formation and detachment from a pore or capillary can be used to improve many industrial processes, including chemical reactions, and combustion and emulsification processes. Drops can, for instance, be formed in processes involving microchannels, a nozzle or the pores in a membrane. Although the drops thus formed commonly disperse into another immiscible liquid flowing past the forming drop, few models focus on liquid drop formation in a cross-flowing immiscible liquid, as was the case in this study.

The creation of drops from a capillary involves two main steps: (1) drop formation, in which the dispersed phase is forced out of the capillary, and the drop grows at the capillary opening, and (2) detachment, when the drop forms a neck, detaches from the dispersed phase and moves with the surrounding continuous phase. Two possible mechanisms are suggested in the literature for the detachment step: *spontaneous transformed based* droplet formation, in which the drops detach because of the minimization of free energy (Sugiura et al. 2001, Yasuno et al. 2002, Rayner et al. 2004), and *shear-induced* droplet formation, in which the detachment is influenced by the cross-flow of the continuous phase (Schröder et al. 1998, Joscelyne and Trägårdh 1999, Wang et al. 2000, Kobayashi et al. 2002, Yasuno et al. 2002). In shear-induced formation, detachment is explained by the fact that the continuous phase has considerable viscous effects when flowing tangentially to the capillary opening. The shear stress and pressure gradient resulting from the cross-flow cause a drag and a lift force, which promote drop detachment.

Experimental studies have shown that motion inside the forming drop can contribute to drop formation and detachment during cross-flow. As the continuous phase shears the interface of the growing drop, the dispersed phase inside the forming drop starts to rotate and forms a vortex (Timgren et al.). Hill established long ago the shear effects of a gas cross-flow on the internal motion in a droplet (Hill, 1894). More recent experimental and numerical studies of a free liquid sphere in an air stream show that the internal motion in the drop is dependent on the direction of the surrounding air stream (Megaridis et al. 1994). Antar and El-Shaarawi (2002a, 2002b and 2004) have presented several numerical studies on the boundary-layer flow around a liquid sphere in an external flow of air, and the effects of viscosity ratio, internal motion and Reynolds number on the local shear stress. They found that shear stress increased with increasing viscosity ratio and spin parameter, and decreasing Reynolds number. The involvement of this internal motion in the drop detachment process remains, however, unexplained.

The formation and detachment of a liquid drop in an immiscible liquid have been modelled with computational

fluid dynamics (CFD) by a number of researchers. Kobayashi et al. (2004 and 2006) investigated the impact of pore geometry and the flow of the dispersed phase on the necking and size of droplets (30-70 µm in diameter) formed in a stagnant continuous phase, and found that detachment occurs inside an elliptic pore if the aspect ratio exceeds 3.5. In order to improve the design of a membrane for membrane emulsification Abrahamse et al. (2001) simulated drop formation in a 5 µm cylindrical pore in laminar cross-flow. They found that the pressure drop over the pore and the velocity in the pore decreased when a neck was formed on the growing droplet and the drop detached above the pore opening. Drops formed from larger nozzles, 0.5-4 mm, have been simulated by, among others, Ohta et al. (1995 and 2003) and Schönfeld and Rensink (2003). However, no one has, as far as we know, focused on the velocity pattern inside and around the forming drop, induced by the cross-flow of a continuous phase. To remedy this, the drop formation from a capillary with a diameter of 200 µm was studied here.

The aim of this work was to describe the effect of the flow of the continuous and the dispersed phases on the shear stress at the drop interface when a drop is formed at a single pore with a circular cross section in a laminar cross-flow. We also discuss the influence of the angular velocity and internal momentum in the drop on the detachment of the drop. Furthermore, the affect of pressure inside and around the forming drop is discussed. For this purpose a commercial CFD code and the volume of fluid (VOF) method were used.

2 Method

The CFD software Fluent 6.2.16 (Fluent Inc., 2005) was used to simulate the formation and detachment of a silicon oil drop into a cross-flowing continuous phase of water and glycerol. Fluent uses a control-volume-based technique to convert the governing equations into algebraic equations that can then be solved numerically. The governing equation used was the mass conservation equation for each phase and the momentum equation.

2.1 Model design

The three-dimensional geometry of the channel and capillary, and the meshes of the fluid volumes were generated using Gambit 2.2.30 (Fluent Inc., 2004). The capillary, which has a circular cross sectional diameter of 0.2 mm and a length of 15 mm, is connected to a channel with a length, height and width of 4×5×4 mm, respectively, see Figure 1.

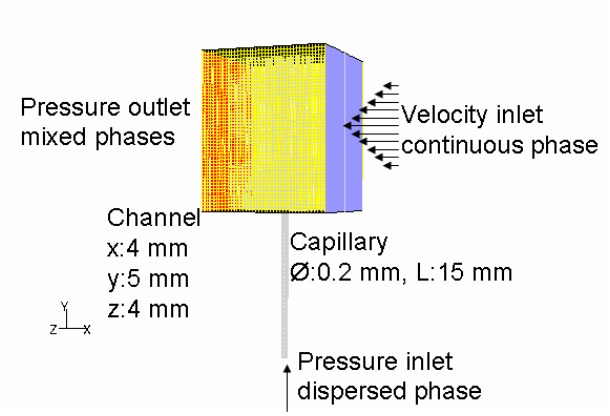

Figure 1: Geometry and boundary settings of the model.

The Cartesian coordinates have their origin at the centre of the capillary opening. The mesh is composed primarily of hexahedral elements, but includes wedge-shaped elements where appropriate. Since a Cooper type scheme was used in Gambit, the volume mesh is based on specified source faces and the capillary opening is one of these faces, which results in a finer mesh in the channel just above the capillary. A hexahedral mesh was selected on the grounds that the calculations of surface tension effects are more accurate with this mesh than with a triangular or tetrahedral mesh. Mesh refinement was adopted in Fluent in order to increase the resolution of the drop formation area. The refinement has the shape of a sphere with a radius of 1 mm and the centre point at (-0.5, 0.4, 0) mm. The grid independence was checked using four different grid sizes. The ratios of the total height of the channel ($h_{channel}$) to the height of a cell in the refined sphere (h_{cell}) were 20, 50, 100 and 200. The errors between the grid sizes were calculated for values of the average velocity in the capillary opening, and the pressure and angular velocity inside the forming drop after half the drop formation time (Table 1). An error of less than 1% was found between the two finest grids, and since the computer time required for the simulation of one drop increased from 13 days to 42 days the second finest grid was chosen.

Silicon oil was assumed to be the dispersed phase and a mixture of water and glycerol the continuous phase. The densities and viscosities of the dispersed and continuous phases are 960 and 1131 kg/m3 and 48 and 6.7 mPa s, respectively. The fluids are assumed to be incompressible and isothermal.

Table 1: Errors when using different grid sizes.

Grid ratio $h_{channel}/h_{cell}$	Capillary velocity (mm/s)	Error (%)	Angular velocity (s^{-1})	Error (%)	Drop pressure (Pa)	Error (%)
20	10.53	1.22	46.0	7.44	165	2.94
50	10.66	2.29	49.7	13.7	167	1.76
100	10.91	0.18	43.7	0.46	170	0
200	10.93		43.5		170	

The boundary conditions are illustrated in Figure 1 and described below with the following initial conditions.

- The entrance of the channel was defined as velocity inlet with a user-defined function (UDF) as initial condition. The UDF is a laminar velocity profile in the y-direction with a maximum velocity ($U_{c,max}$) of 0.20 m/s at y=2.5 mm.
- The entrance of the capillary was defined as pressure inlet with a constant gauge pressure on the disperse phase. The gauge pressure was set to 7000 Pa. A constant pressure was used instead of a velocity condition since a constant pressure is applied on the dispersed phase in our experimental study (Timgren et al.).
- The outflow of the channel was defined as pressure outlet with zero gauge pressure. The operating pressure was set to atmospheric pressure.
- The side walls of the channel were defined as symmetry since the real channel used in the experimental study had a width of 20 mm. Thus, the velocity at these walls follows the velocity profile defined at the channel entrance, which can be assumed to be correct since the axial velocity profile in the horizontal plane is flat in the rectangular channel used.
- All other walls are assumed to be stationary with a no-slip boundary condition, and a contact angle of 179°.

2.2 Numerical methods

The segregated solver for an unsteady laminar flow was used in Fluent and the volume of fluid method was used to track the interface between the oil drop and the continuous phase. The VOF model is a surface-tracking technique that is useful when studying the position of the interface between two immiscible fluids. A single set of momentum equations is shared by the fluids, and the volume fraction of each of the fluids in each computational cell is tracked throughout the domain. The VOF model uses phase averaging to define the amount of continuous and dispersed phase in each cell. A variable, α, was defined as:

$\alpha = 1 \Rightarrow$ when the cell is 100% filled with continuous phase

$\alpha = 0 \Rightarrow$ when the cell is 100% filled with dispersed phase

$0 < \alpha < 1 \Rightarrow$ when the cell contains an interface between the two phases

and the density, ρ, and viscosity, μ, for the two phases (1 and 2) can be calculated using a linear dependence:

$$\rho = \rho_1 \alpha + \rho_2 (1- \alpha) \quad (1)$$

$$\mu = \mu_1 \alpha + \mu_2 (1- \alpha) \quad (2)$$

There are several different VOF algorithms with different accuracies and complexities in Fluent and the geometric reconstruction scheme used in this study is based on the work of Youngs (1982) and further described by Rudman (1997). This scheme permits a piecewise-linear approach, which assumes that the interface has a linear slope within each cell, and the position of the interface is calculated from the volume fraction and its derivatives in the cell.

The solutions of the velocity field and pressure are calculated using a body-force-weighted discretization scheme for the pressure, the Pressure-Implicit with Splitting of Operators (PISO) scheme for the pressure-velocity coupling and a power law scheme is used for the momentum calculation. The body-force-weighted scheme is used since it works well with the VOF model, and the PISO scheme is chosen to improve the efficiency of the calculation of the momentum balance after the pressure-correction equation is solved. The convergence limit was set to a residual sum of 10^{-3} for the continuity and velocity components. The time step was set to 10^{-5} s.

3 Results and Discussion

3.1 Drop formation

Figure 2 shows the simulated contours in the centre cross section of the formation of an oil drop at the capillary opening at four points in time. The forming drop was shown to be affected by the cross-flow of the continuous phase. The diameter of the drop increased and eventually a neck was formed above the capillary opening. The drop continued to grow and the neck diameter decreased until the drop detached at a final size of nearly 1 mm. A small volume of the oil phase remained attached to the capillary opening from which the next drop started to form.

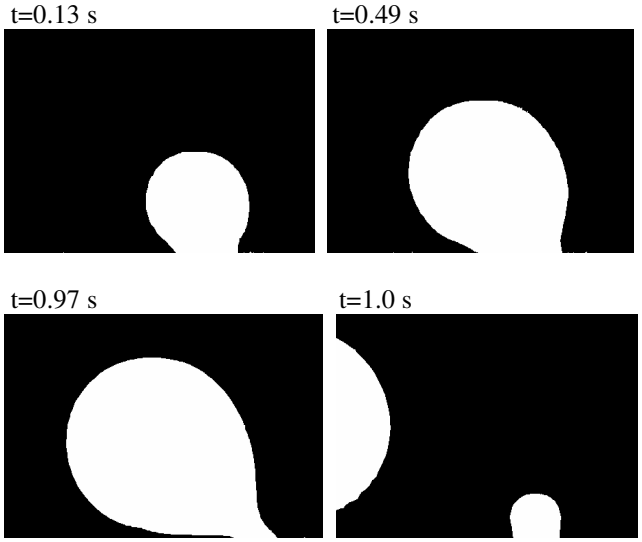

Figure 2: Contours of a silicon oil drop formed and detached in a continuous water/glycerol phase cross-flowing from right to left with a maximum velocity ($U_{c,max}$) of 0.20 m/s. The pressure applied to the oil phase is 7000 Pa.

3.2 Capillary velocity

The variation of the oil velocity at the capillary opening and the pressure inside the centre of the forming drop are shown in Figure 3. The pressure in the drop corresponds to the Laplace pressure, which is inversely proportional to the radius of a drop curvature. This results in a large pressure at the beginning of the drop formation process, and also at the end when the neck has been formed. As can be seen, the capillary velocity is not only affected by the constant pressure applied to the oil phase, but also by the pressure caused by the cross-flow above the capillary opening and, above all, by the pressure inside the drop.

The maximum velocity in the capillary was observed just before the neck was formed, when the curvature of the drop interface was at a maximum. The oil phase had a minimum velocity in connection with detachment. Immediately before detachment the amount of oil between the neck and the capillary opening was small. In addition, this fraction of the oil was deformed, thus indicating that the radius could be assumed to be very small and therefore also result in a large pressure. The velocity increases again after detachment as an effect of the reorientation of the oil remaining at the capillary opening. The remaining deformed oil rest returns to a smooth shape, which decreases the pressure and increases the flow of oil out of the capillary. As the new drop grows the pressure will further decrease and hence the capillary velocity will increase. This indicates that the pressure inside the forming drop has the largest effect on the velocity variations in the oil phase. Abrahamse et al. (2001) presented similar results, although they used a pore diameter of 5 µm in their simulations.

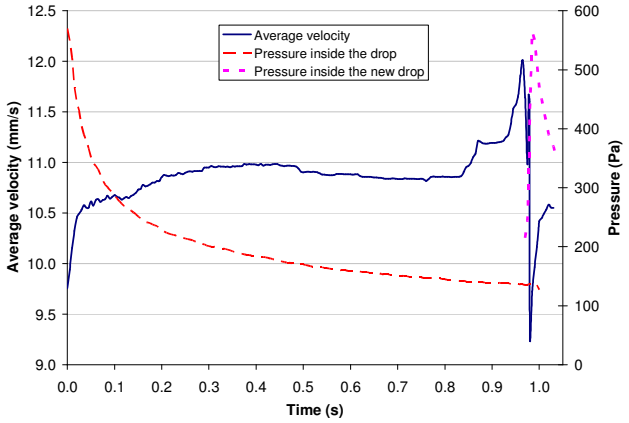

Figure 3: Average velocity in the silicon oil at the capillary opening and the pressure inside the forming drop. Drop detachment occurs at t=0 and t=0.98 s.

3.3 Velocity pattern inside the drop

The simulated velocity field in the centre cross section of a forming drop can be compared to a large vortex, as can be seen in Figure 4. This vortex formation was obviously induced by the shear arising from the cross-flow of the continuous phase. As the drop approached detachment, the centre of the vortex moved towards the lower left part of the drop and the velocity vectors straightened out in the free drop following the continuous phase.

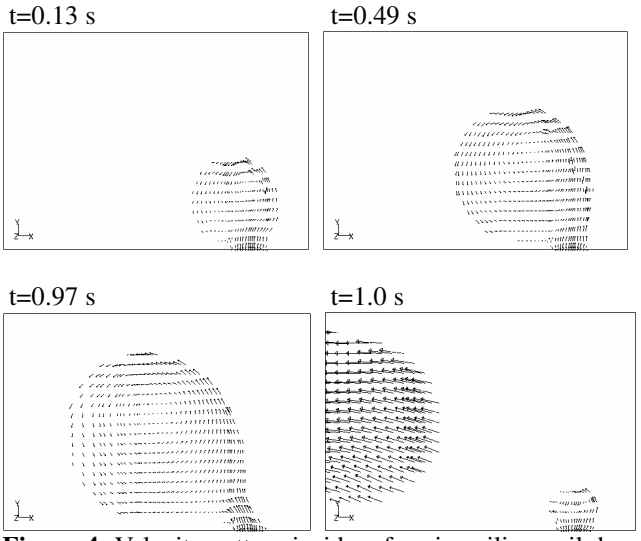

Figure 4: Velocity pattern inside a forming silicon oil drop in water/glycerol cross-flowing from right to left with $U_{c,max}$=0.20 m/s. The pressure applied to the oil phase is 7000 Pa.

The circulation inside the drop changes during drop formation and a method of measuring this is to determine the angular velocity, which is a measure of the rotation of a fluid element as it moves in the flow field. Figure 5 shows how the calculated average angular velocity in the whole drop changes as the drop grows and finally detaches at t=0.98 s.

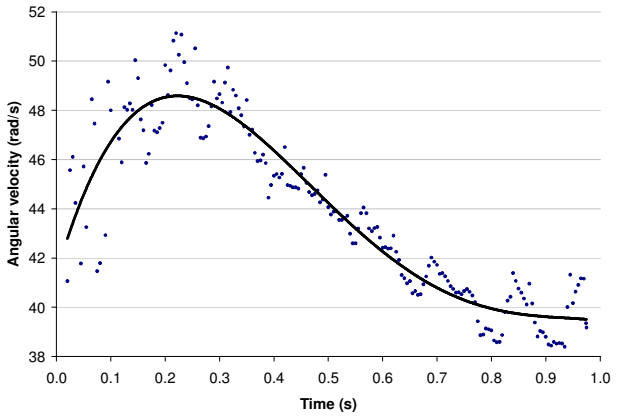

Figure 5: Average angular velocity in the forming oil drop, which detaches at t=0.98 s.

The angular velocity increases during the first fifth of the drop formation time since the drop is relatively small when the influence of the cross-flow starts to affect the drop. In addition, at the beginning of drop formation, the oil flux from the capillary influences the motion in the drop, thus affecting the amplitude of the angular velocity. As the drop continues to grow the influence of the cross-flow will increase, but since the drop radius also increases the net result will be a decrease in the average angular velocity. A steady state is approached as the point of drop detachment approaches, which indicates that the shear resulting from the cross-flow has a greater effect than during the decreasing angular velocity phase. The spread of the data during the early part of drop formation is mainly due to the location of the interface of the drop in relation to the grid cells. This problem is more pronounced when the drop is small and the number of cells occupied by the dispersed phase is limited.

The internal rotation may have a minor influence on drop detachment, but the drop will apparently detach when a steady state is approached. However, the analysis of angular velocity provides insight into the fluid transport within drops, which is important for mixing efficiency when the dispersed phase consists of an emulsion or several components, for example, surfactants or an active substance.

3.4 Velocity field around the drop

The flow of the continuous phase around the forming drop is shown in Figure 6. There is a stagnation point at the front of the drop, where a boundary layer begins to grow. It then follows the interface around the drop until a separation can be seen behind the drop.

The Reynolds number (Re_d), calculated with respect to the curvature of the drop and the free flow velocity in the continuous phase at half the height of the drop, increases from 1 to approximately 20 as the drop grows. Separation occurs at the rear of the drop, and between the forming drop and the channel wall, both in this simulated study and in our experimental study (Timgren et al.), which may be due to a local interaction caused by the motion inside the drop. The circulation in the drop, induced by the oil flux in the capillary and the shear from the cross-flow, has a higher velocity than the continuous phase behind the drop. This difference in velocity leads to a shear from the oil on the surrounding continuous phase downstream of the drop. Others have also shown that separation occurs earlier with increased viscosity ratio (internal to external phase). The viscosity ratio in the present study is 7.2, which is higher than the conditions in the study by Antar and El-Shaarawi (2002a). The onset of separation is dependent on the viscosity ratio since this affects the velocities in the boundary layer outside the drop.

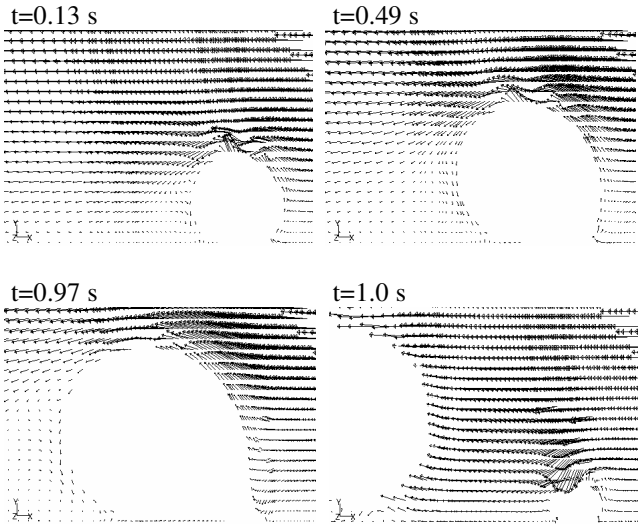

Figure 6: Velocity pattern in the continuous water/glycerol phase around a forming silicon oil drop. The cross-flow is from right to left with $U_{c,max}$=0.20 m/s. The pressure applied to the oil phase is 7000 Pa.

3.5 Shear stress at the interface

The cross-flow of the continuous phase is found to induce a shear at the interface of the forming drop, and the calculated shear stress in the two phases at t=0.49 s and t=0.97 s in the formation process is presented in Figure 7. The centre point in the cross section of the drop is defined as the point at half the height and width of the drop. The shear stress inside the drop has a higher value than that outside, mainly because the relatively high velocity of the jet from the capillary affects the calculated shear stress, which is more pronounced for the smaller drop at t=0.49 s. The results show a maximum shear stress in both phases upstream above the forming drop at angles of about 75º (also 45º in Figure 7a) and 60º for the inside and outside of the drop, respectively. This corresponds well with the results of Antar and El-Shaarawi (2002a), which showed a shear stress maximum in the surrounding phase at 60º from the stagnation point.

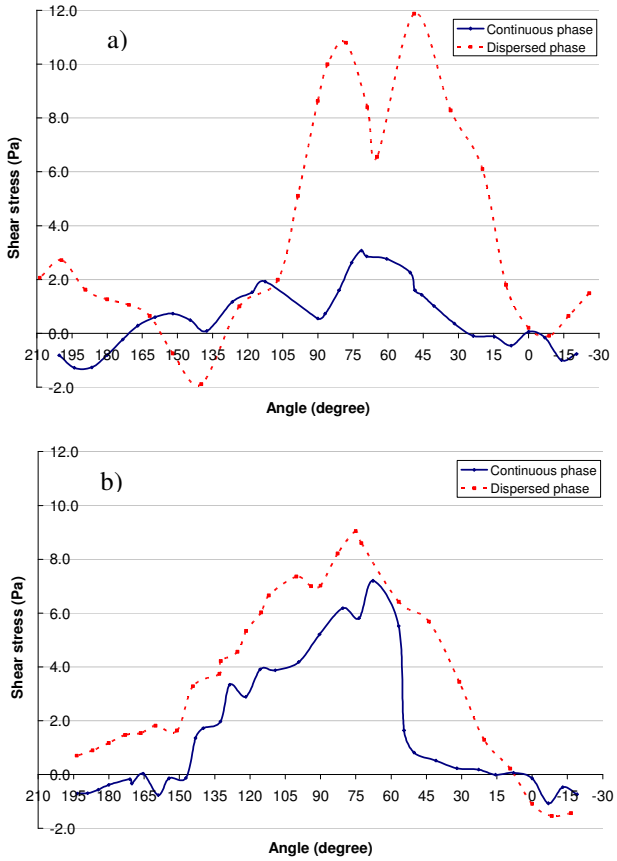

Figure 7: Shear stress at the interface inside (dispersed phase) and around (continuous phase) a forming drop. The front (right side) of the forming drop is at 0º, the top at 90º and the back (left side) at 180º. The time is a) t=0.49 s and b) t=0.97 s.

The peak at 45º in the dispersed phase in Figure 7a is due to the jet of oil from the capillary. This is the point where the interface of the drop is straight above the centre of the capillary opening which leads to a large velocity vector next to the interface. The following decline in shear stress is an effect of the curvature of the drop, and the shear stress from the continuous phase causes after that another peak in the dispersed phase. Immediately after the maximum, a major decrease in shear stress occurs in both phases since the cross-flow partly separates from the interface. This phenomenon is more pronounced as the drop grows and the Reynolds number (Re_d) increases. There are also negative values of shear stress at the front of the drop at angles near zero, where the cross-flow meets the forming drop, caused by the high flux in the oil phase and also by the fact that the cross-flow has a stagnation point at this position. The definition of the stagnation point is the point at which the velocity normal to the interface is zero, hence the point at which the shear stress in the continuous phase intersects the angle-axis.

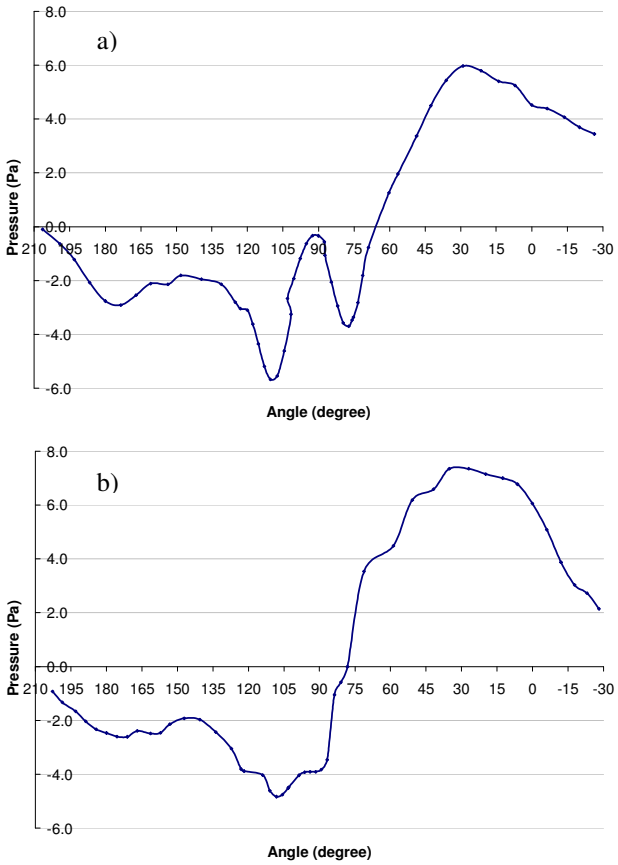

Figure 8: Pressure field around a forming drop. The front (right side) of the forming drop is at 0º, the top at 90º and the back (left side) at 180º. The time is a) t=0.49 s and b) t=0.97 s.

3.6 Pressure field around the drop

The pressure field in the surrounding continuous phase has a major influence on the whole process of drop formation and detachment as it causes the drop to lift and lean in the direction of the cross-flow. The pressure in Figure 8 is expressed relative to the operating pressure, which is set to atmospheric pressure. The results in Figure 8 show that the highest pressures are found at 30º, which corresponds to a location near the stagnation point and a low positive shear stress in the continuous phase. In addition, the lowest pressures are seen at 110º, where the surrounding flow starts to separate from the interface of the drop. The pressure peak at 90º in Figure 8a, corresponding to a decline in shear stress found in Figure 7a, is probably caused by the irregular velocities in the continuous phase at the top of the drop at t=0.49 s (shown in Figure 6), which in turn is due to the high local drop expansion rate. The maximum in the pressure field increases as the drop grows, as can be seen when Figure 8a and b are compared. This is caused by the higher velocity and shear stress, resulting from the cross-flow, which affects the drop.

4 Conclusions

Numerical simulation of drop formation at a single capillary with a diameter of 200 µm in a horizontal cross-flow shows that the pressure inside the forming drop affects the velocity of oil leaving the capillary. A high internal pressure causes a decreased average velocity at the capillary opening. The flow of the surrounding continuous phase induces a shear at the interface of the drop, which results in rotational motion inside the oil drop. The shear stress at the interface has its origin not only in the cross-flow but also in the flow of oil out of the capillary. The effect of the flow of oil is more pronounced in the beginning of the formation of a drop. The shear stress outside the drop causes a drag which, together with the drag originated from the pressure field around the drop, promotes drop detachment.

Acknowledgements

This work was financially supported by the Swedish Research Council.

References

Abrahamse, A.J., van der Padt, A. & Boom, R.M. Process fundamentals of membrane emulsification: Simulation with CFD. AIChE Journal, Vol. 47, 1285-1291 (2001)

Antar, M.A. & El-Shaarawi, M.A.I. Effect of viscosity ratio, spin and Reynolds number on the flow characteristics about a liquid sphere in a gas stream. International Journal of Numerical Methods for Heat & Fluid Flow, Vol. 12, 800-816 (2002a)

Antar, M.A. & El-Shaarawi, M.A.I. Mixed convection around a liquid sphere in an air stream. Heat and Mass Transfer, Vol. 38, 419-424 (2002b)

Antar, M.A. & El-Shaarawi, M.A.I. Simultaneous effect of rotation and natural convection on the flow about a liquid sphere. Heat and Mass Transfer, Vol. 40, 393-399 (2004)

Hill, M.J.M. On a spherical vortex. Philosophical Transactions of the Royal Society of London. A, Vol. 185, 213-245 (1894)

Joscelyne, S.M. & Trägårdh, G. Food emulsions using membrane emulsification: conditions for producing small droplets. Journal of Food Engineering, Vol. 39, 59-64 (1999)

Kobayashi, I., Yasuno, M., Iwamoto, S., Shono, A., Satoh, K. & Nakajima, M. Microscopic observation of emulsion droplet formation from a polycarbonate membrane. Colloids and Surfaces A: Physicochemical and Engineering Aspects, Vol. 207, 185-196 (2002)

Kobayashi, I., Mukataka, S. & Nakayima, M. CFD simulation and analysis of emulsion droplet formation from straight-through microchannels. Langmuir, Vol. 20, 9868-9877 (2004)

Kobayashi, I., Uemura, K. & Nakajima, M. CFD study of the effect of a fluid flow in a channel on generation of oil-in-water emulsion droplets in a straight-through microchannel emulsification. Journal of Chemical Engineering of Japan, Vol. 39, 855-863 (2006)

Megaridis, C.M., Hodges, J.T., Xin, J., Day, J.M. & Presser, C. Internal droplet circulation induced by surface-driven rotation. International Journal of Heat and Fluid Flow, Vol. 15, 364-377 (1994)

Ohta, M., Yamamoto, M. & Suzuki, M. Numerical analysis of a single drop formation process under pressure pulse conditions. Chemical Engineering Science, Vol. 50, 2923-2931 (1995)

Ohta, M., Iwasaki, A., Obata, E. & Yoshida, Y. A numerical study of the motion of a spherical drop rising in shear-thinning fluid systems, Journal of Non-Newtonian Fluid Mechanics, Vol. 116, 95-111 (2003)

Rayner, M., Trägårdh, G., Trägårdh, C. & Dejmek, P. Using the Surface Evolver to model droplet formation processes in membrane emulsification. Journal of Colloid and Interface Science, Vol. 279, 175-185 (2004)

Rudman, M. Volume-tracking methods for interfacial flow calculations. International Journal for Numerical Methods in Fluids, Vol. 24, 671-691 (1997)

Schröder, V., Behrend, O. & Schubert, H. Effect of dynamic interfacial tension on the emulsification process using microporous, ceramic membranes. Journal of Colloid and Interface Science, Vol. 202, 334-340 (1998)

Schönfeld, F. & Rensink, D. Simulation of droplet generation by mixing nozzles. Chemical Engineering and Technology, Vol. 26, 585-591 (2003)

Sugiura, S., Nakajima, M., Iwamoto, S. & Seki, M. Interfacial tension driven monodispersed droplet formation from microfabricated channel array. Langmuir, Vol. 17, 5562-5566 (2001)

Timgren, A., Trägårdh, G. & Trägårdh, C. Application of the PIV technique to measurements around and inside a forming drop in a liquid-liquid system. Manuscript

Wang, Z., Wang, S., Schröder, V. & Schubert, H. Effect of continuous phase viscosity on membrane emulsification. Chinese Journal of Chemical Engineering, Vol. 8, 108-112 (2000)

Yasuno, M., Nakajima, M., Iwamoto, S., Maruyama, T., Sugiura, S., Kobayashi, I., Shono, A. & Satoh, K. Visualization and characterization of SPG membrane emulsification. Journal of Membrane Science, Vol. 210, 29-37 (2002)

Youngs, D.L. Time-dependent multi-material flow with large fluid distortion. In Numerical Methods for Fluid Dynamics, 273-285 (1982)